solution series are desirable for elucidating further details of the phase transition.

We would like to thank Professors H. Minato and T. Sugimura for helpful suggestions, Drs N. Haga and F. Nishi for valuable discussions and Mr K. Oyobe for his assistance in drawing the figures. We thank the Ministry of Education, Science and Culture for supporting the leave of HO to carry out this work for a year at the Mineralogical Institute, Faculty of Science, University of Tokyo.

References

BOND, W. L. (1951). *Rev. Sci. Instrum.* **22**, 344–345.
BROWN, G. E., SUENO, S. & PREWITT, C. T. (1973). *Am. Mineral.* **58**, 619–697.
BUSING, W. R., MARTIN, K. O. & LEVY, H. A. (1963). *RADY.* Report ORNL-TM-305. Oak Ridge National Laboratory, Tennessee, USA.
FISCHER, R. X. & TILLMANNS, E. (1983). *Neues Jahrb. Mineral. Monatsh.* **2**, 49–59.
FISCHER, R. X. & TILLMANNS, E. (1984). *Z. Kristallogr.* **166**, 245–256.
FISCHER, R. X. & TILLMANNS, E. (1987). *Acta Cryst.* C**43**, 1852–1854.
IKAWA, H., OTAGIRI, T., IMAI, O., SUZUKI, M., URABE, K. & UDAGAWA, S. (1986). *J. Am. Ceram. Soc.* **69**, 492–498.
International Tables for X-ray Crystallography (1974). Vol. IV. Birmingham: Kynoch Press. (Present distributor Kluwer Academic Publishers, Dordrecht.)
JOHNSON, C. K. (1965). *ORTEP.* Report ORNL-3794. Oak Ridge National Laboratory, Tennessee, USA.
LIEBAU, F. (1985). *Structural Chemistry of Silicates,* pp. 24–30. Berlin: Springer-Verlag.
MAKI, I. & SUGIMURA, T. (1968). *Yogyo Kyoukai Shi,* **76**, 144–148.
OHSATO, H., MAKI, I. & TAKÉUCHI, Y. (1985). *Acta Cryst.* C**41**, 1575–1577.
OHSATO, H., TAKÉUCHI, Y. & MAKI, I. (1986). *Acta Cryst.* C**42**, 934–937.
TAKÉUCHI, Y., NISHI, F. & MAKI, I. (1980). *Z. Kristallogr.* **152**, 259–307.
TAKÉUCHI, Y., YAMANAKA, T., HAGA, N. & HIRANO, M. (1984). *Materials Science of the Earth's Interior,* edited by I. SUNAGAWA, p. 191 Tokyo: Terrapub.
TAYLOR, D. (1984). *Mineral. Mag.* **48**, 65–79.
TOKONAMI, M. (1965). *Acta Cryst.* **19**, 486.

Acta Cryst. (1990). B**46**, 131–138

Structure, Electron Density and Thermal Motion of $KCuF_3$

BY R. H. BUTTNER, E. N. MASLEN AND N. SPADACCINI

Department of Physics, University of Western Australia, Nedlands, WA 6009, *Australia*

(*Received* 30 *January* 1989; *accepted* 9 *October* 1989)

Abstract

Thermal parameters from a refinement with newly collected data for $KCuF_3$ [$M_r = 159{\cdot}64$, tetragonal, $I4/mcm$, $a = b = 5{\cdot}8569\ (6)$, $c = 7{\cdot}8487\ (8)$ Å, $V = 269{\cdot}24\ (6)$ Å^3, $Z = 4$, $D_x = 3{\cdot}938$ Mg m^{-3}, λ(Mo $K\alpha$) $= 0{\cdot}71069$ Å, $\mu = 9{\cdot}747$ mm^{-1}, $F(000) = 300$, $T = 298$ K, final $R = 0{\cdot}020$, $wR = 0{\cdot}014$ for 655 unique reflections] are consistent with those from a reanalysis of previously published data with a revised model including an isotropic extinction correction. There are two distinct types of F atoms and three different Cu—F bonds. The amplitude of the Cu—F2 stretching mode is largest for the long Cu—F2 bond. The single refined positional parameter differs significantly from previous determinations but the difference is shown to be due to bias in the redistribution of bonding electron density. Its value from refinement with full data gives a more satisfactory description of the net force at equilibrium geometry than that based on high-angle refinement. Effective atomic charges for Cu, K and F2, calculated by partitioning the difference density, are consistent with those in related structures but F1 is positively charged. This is explained by the strong depleting effect of exchange on the electron density, owing to structural compression along the c axis. The positive charge on F1 accounts for changes in K—F and F—F distances from the ideal perovskite values. There is excess electron density of $1{\cdot}61$ e Å^{-3} located $0{\cdot}45$ Å from F2, indicating strong dipole polarization along the Cu—F2—Cu bond. The shape of the depletion of electron density near Cu is broadly compatible with that expected for a cooperative Jahn–Teller distorted Cu system, but its radial dependence suggests depletion of paired spins along the shorter Cu—F bonds and of unpaired spins along the longest Cu—F bond.

Introduction

$KCuF_3$ contains atoms with moderate atomic number enabling its electron density to be measured

0108-7681/90/020131-08$03.00

with good precision. Difference densities for $KCuF_3$ were evaluated by Tanaka, Konishi & Marumo (1979) and Tanaka & Marumo (1982) (referred to as study I), complementing investigations of $3d$-spin repopulation in the isomorphic cubic KMF_3 series, where M = Mn, Fe, Co and Ni (Kijima, Tanaka & Marumo, 1981, 1983; Miyata, Tanaka & Marumo, 1983). While $KCuF_3$ is not strictly isomorphous, its structure is closely related to the ideal perovskite series. The equivalent cubic perovskite cell for $KCuF_3$ has $a_{eq} = (V/4)^{1/3} = 4{\cdot}0678$ (3) Å. Jahn–Teller distortion associated with the Cu d^9 state (Kanamori, 1960) displaces the octahedrally coordinated F atoms, resulting in short (Cu—F2), medium (Cu—F1) and long (Cu—F2) bonds as shown in Fig. 1.

The data from study I have been reanalyzed by Spadaccini (1988) (referred to as study II), preferring isotropic extinction to the anisotropic model applied in the original analysis. Additional data, kindly supplied by the authors of study I, were helpful in that work. The $\Delta\rho$ map is strongly influenced by extinction, and it may be difficult to distinguish real features from artifacts in a single experiment. Therefore an independent data set was collected from a crystal of type 'a', as defined by Okazaki (1969a,b), and described more fully by Hutching, Samuelsen, Shirane & Hirakawa (1969). The results are compared below with that of study II paying particular attention to properties likely to be typical of the series as a whole.

Because the Jahn–Teller distortion of the Cu atom in this structure resembles that in the high-T_c superconducting perovskite structures, $KCuF_3$ models some aspects of high-T_c superconductivity. The conclusions have been applied to help elucidate the role of $\Delta\rho$ in the more-difficult-to-crystallize superconducting compound $YBa_2Cu_3O_{7-x}$ (Buttner, Maslen & Spadaccini, 1990).

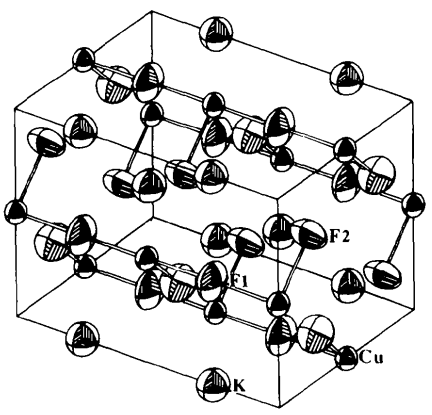

Fig. 1. The $KCuF_3$ type 'a' cell structure with vibrational ellipsoids plotted at the 99% probability level.

Experimental

The crystals for study I were grown from the melt. Those for this study were grown from solution by a method for preparing well-faceted, single-domained specimens described by Kadota, Yamada, Yoneyama & Hirakawa (1967). Small specimens which were almost colourless were shown by Weissenberg photographs to be disordered and twinned. The better samples were a pale-violet colour but were too large ($> 0{\cdot}2 \times 0{\cdot}2 \times 0{\cdot}2$ mm) for an accurate electron density study. A specimen suitable for accurate data collection was cleaved. The fragment forms an approximate trapezium-based prism with a (221), two (001) and three (110) faces. Its volume of $6{\cdot}72 \times 10^{-4}$ mm^3 is comparable with that of the spherical specimen used in study I. Cell dimensions were determined from six reflections ($29 < \theta < 33°$).

The data were collected on an Enraf–Nonius diffractometer using Mo $K\alpha$ radiation. Experimental details are given in Table 1. A sphere of data with $\sin\theta/\lambda < 1{\cdot}28$ Å^{-1} was measured. The 8904 intensities were corrected analytically for absorption (Alcock, 1974), sorted and merged, yielding 655 independent reflections. After corrections for Lorentz and polarization factors all were included in the structure refinement using full-matrix least squares based on F. The reference state for all structure-factor calculations was the independent-atom model (IAM). Atomic scattering factors were taken from Cromer & Mann (1968) and anomalous-dispersion corrections from Cromer & Liberman (1970). A scale factor, extinction parameter and 11 structural parameters, allowed by site symmetry, were determined. On the basis of structure-factor agreement the isotropic extinction model of Zachariasen (Larson, 1970) was preferred to the alternatives (Becker & Coppens, 1974). The average $\overline{T}$ for each set of equivalent reflections was used in correcting for extinction (minimum extinction $y = 0{\cdot}63$, with six reflections having $y < 0{\cdot}8$). Refinement details are included in Table 1, with final positional and thermal parameters in Table 2. All calculations utilized the *XTAL* system of crystallographic programs (Hall & Stewart, 1988).*

In study I the weak reflections were culled by applying the 'less than' criterion $|F_o| < 3\sigma(|F_o|)$, with $\sigma(|F_o|)$ determined from counting statistics. The 220 reflection was also omitted in view of the large difference between F_o and F_c ($F_o = 145{\cdot}75$, $F_c = 198{\cdot}72$). The strong anisotropy in extinction reported for $KCuF_3$ is not consistent with the other perovskites where the extinction is dominated by the

* Lists of structure factors have been deposited with the British Library Document Supply Centre as Supplementary Publication No. SUP 52376 (3 pp.). Copies may be obtained through The Technical Editor, International Union of Crystallography, 5 Abbey Square, Chester CH1 2HU, England.

Table 1. *Experimental and refinement data*

Diffractometer	CAD-4
Monochromator	Graphite
Scan type	$\omega/2\theta$
Scan speed	8·24° min^{-1}
Peak scan width ($a + b \tan\theta$)	0·5; 0·34°
Max. 2θ	129·7°
Max. variation in intensity of standards ± (800) ± (080) ± (0,0,12)	0·9%
No. of reflections measured ($-14 \le h \le 14$, $-14 \le k \le 14$, $-18 \le l \le 19$)	8904
Transmission range in absorption corrections	0·42–0·65
R_{int} (before and after absorption)	0·099; 0·029
No. of independent reflections ($0 \le h \le 10$, $0 \le k \le 14$, $0 \le l \le 19$)	655
R	0·020
wR	0·014
S	3·24 (9)
Weights	$1/\sigma^2(F_o)$
Final max. shift/e.s.d.	0·00002
Max. height in final difference Fourier synthesis	1·61 (9) e Å^{-3}
Min. height in final difference Fourier synthesis	−1·56 (7) e Å^{-3}

Table 2. *Atomic coordinates and anisotropic thermal parameters* (Å^2 × 10^5)

Cu at (0, ½, 0), K at (0, 0, ¼), F1 at (0, ½, ¼) and F2 at (x, x + ½, 0). Temperature factors given by $T = \exp\{2\pi^2[(h^2 + k^2)a^{*2}U_{11} + l^2c^{*2}U_{33} + 2hka^*b^*U_{12}]\}$.

	x	U_{11}	U_{33}	U_{12}	U_{eq}†
Cu		788 (3)	616 (3)	−141 (4)	730 (2)
K		1575 (5)	1474 (8)	0	1541 (4)
F1		2295 (21)	743 (20)	0	1780 (12)
F2	0·22803 (7)	1478 (14)	2049 (27)	−580 (17)	1668 (11)
		U'_{11} [$\bar{1}$10]	U'_{22} [110]	U'_{33} [001]	
Cu		929 (5)	647 (5)	616 (3)	
F2		2058 (22)	898 (22)	2049 (27)	

†$U_{eq} = (U_{11} + U_{22} + U_{33})/3$.

isotropic term (Maslen & Spadaccini, 1989). Furthermore the small spread in the intensities of equivalent reflections (R_{int} = 0·009) before extinction corrections suggests it is essentially isotropic.

Study II included the strong 220 reflection, but no additional data were available for the weak reflections. Refinement of an isotropic extinction correction (Larson, 1970) resulted in a minimum extinction of y = 0·71 and the residual indices of R = 0·015, wR = 0·018 and S = 4·02, with refined parameters as set out in Table 3. The thermal parameters obtained in study II differ little from those of study I (or from those of this study, as reflected in the agreement between Tables 2 and 3). However, the topology of $\Delta\rho$ near the Cu atom was very different. The $\Delta\rho$ maps were more consistent with those of the other members of the series, confirming the improvement in the extinction model.

The refined x coordinates for F2 in Tables 2 and 3 differ significantly. Any explanation of this discrepancy in terms of the uncertainty in position, indicated by the standard deviations in one or both of the analyses being unrealistically low, is not reasonable in view of the high degree of consistency between the thermal parameters, which exceeds that normally achieved in independent structure refinements.

Table 3. *Structural parameters from study* II

Parameters are defined as in Table 2.

	x	U_{11}	U_{33}	U_{12}	U_{eq}
Cu		784 (4)	606 (4)	−160 (10)	725 (2)
K		1561 (8)	1450 (10)	0	1524 (5)
F1		2260 (30)	720 (30)	0	1747 (17)
F2	0·22756 (10)	1400 (20)	1980 (40)	−610 (30)	1593 (14)

The possibility that differing degrees of disorder could account for the shift in the x coordinate was considered. In that context the existence of polytypes with F2 displaced either systematically, or in disordered arrays (Okazaki, 1969*a*,*b*) is relevant. The difference between these structures relates to the way in which F2 is displaced from the ideal perovskite position at the midpoint of the Cu—Cu vector. In adjacent c layers (*i.e.* $z = 0$, $z = \frac{1}{2}$ *etc.*) the displacements are in opposite directions along the Cu—Cu vector for the type '*a*' structures and are in the same direction in type '*d*' structures.

The amplitude of thermal vibration for F2 along the Cu—F2—Cu vector is larger than that of F1 along Cu—F1—Cu, indicating that the potential for displacement of F2 is a more slowly varying function of distance, at least over the range of values obtained. This is also consistent with Cu vibrating more in this direction than along Cu—F1. Notwithstanding the larger thermal motion of F2, the potential of the region cannot rise too slowly from the mean position. There is no evidence for a dynamic transition between '*a*' and '*c*' type structures, which have space group *P4/mbm* for a cell with a halved c axis (Okazaki, 1969*a*,*b*). Perturbative displacements of F2 must be dampened by changes to the dipole character at F2 in the Cu—F2—Cu interaction (Fig. 3*a*).

Thus the idea that differing degrees of disorder could account for the shift in the x coordinate is only superficially attractive. No evidence for multidomain structures was obtained during photographic work. The dimensions for type '*a*' crystals of 5·8563 (3) and 7·8474 (4) Å are in good agreement with those for the crystal under study, while values for the extreme structural variation, type '*d*', of 5·8542 (3) and 3·9303 (5) Å [$2c$ = 7·8606 (10) Å] differ significantly. It is also very difficult to envisage that thermal parameters could agree so accurately for crystals with different phase compositions.

The Table 2 values were checked by refinement using data with $\sin\theta/\lambda > 0{\cdot}7$ Å^{-1} to 'reduce' any bias resulting from redistribution of bonding electron density, or low-angle extinction-affected data. This revealed a curious drift of the position parameter x from 0·22803 (7) to 0·22745 (6), shifting 0·0048 Å towards the value observed in studies I and II, which were based on less extensive data. Careful scrutiny indicates that the x coordinate varies because of

change in the bias by redistribution of bonding electron density when the reflection weights are altered, as further described below.

Structural geometry

The Cu atom is at the centre of a distorted octahedron formed by six F atoms with the three independent Cu—F bond lengths given in Table 4 and all F—Cu—F angles 90 or 180°. The elongation of one Cu—F2 bond satisfies the prediction of the Jahn–Teller theorem, but inequality between the two shorter bond lengths cannot be explained in terms of the electronic states of Cu and its interactions with F only. If nearest-neighbour interactions alone are significant it is difficult to explain why Jahn–Teller distortion does not induce a simpler D_{4h} distortion of the ideal cubic cell.

The second nearest-neighbour interactions are conveniently compared with those for $KCoF_3$ with a = 4·0688 (7) Å (Kijima *et al.*, 1981), which is close to that of the equivalent cubic cell for $KCuF_3$. The second coordiantion sphere for Cu is formed by eight K atoms located approximately in the [111] direction, with a K—Cu distance of 3·5250 (3) Å close to that of 3·5237 (3) Å for $KCoF_3$. It is thus unlikely that the K—Cu interaction affects the structural reorganization induced by the Jahn–Teller effect.

On the other hand there are striking changes in the lengths of interaction vectors involving the F atoms, as set out in Table 4. In addition to its two nearest-neighbour F—Cu vectors [1·9622 (2) Å], F1 has four tetrahedrally displaced F2 neighbours at 2·7235 (3) Å and four K atoms at 2·9285 (3) Å. These are shorter and longer, respectively, than the corresponding values of 2·0344 (4) Å for F—Co and 2·8771 (3) Å for F—F and F—K in the $KCoF_2$ structure. It is intriguing that the changes for the F2—F2 and F2—K vectors, of lengths 2·9397 (6) and 2·8585 (3) Å, respectively, are in opposite directions to those involving F1. The systematic relationship of these changes to the identity of the contact atoms suggest that there is a chemical difference between F1 and F2 atoms.

The length of the principal axis of the vibration ellipsoid of 0·095 (1) Å for F2 along the bond is markedly longer than the corresponding value of 0·086 (1) Å for F1. This difference is partly clarified by inspection of Fig. 2, where thermal parameters of F1, F2 and U_{eq} for K are compared with those for F and K in the cubic KMF_3 series [M = Mn, Fe, Co, Ni, Maslen & Spadaccini (1989); M = Zn, Buttner & Maslen (1988)]. U_{eq} for Cu is markedly higher than those for M in that series, as expected for a Jahn–Teller distorted atom. For F and K, the observed values notionally assigned to an ideal Cu perovskite unit cell [4·0678 (3) Å] agree fairly well with the values predicted by the general trend for the ideal structures. If the actual Cu—Cu distances were applied when comparing $U_{\parallel}$ values, those for F1 would be displaced to the left [3·9244 (4) Å], with those for F2 moved to the right [4·1415 (7) Å] in Fig. 2. Both are then slightly above the trend line, a result consistent with their bonding to the Jahn–Teller-distorted Cu atom. The fact that $U_{\perp}$ (F1, F2) and U_{eq} for K, which are affected less by the Cu distortion, agree more closely with those of the cubic perovskite series, emphasizes the relationship of these thermal parameters to the global character of the crystal field.

Table 4. *Interaction vector lengths* (Å) *involving* F *in* $KCuF_3$ *(from this study) and in* $KCoF_3$ *(from Kijima et al.* 1981)

		$KCuF_3$		$KCoF_3$
F—Cu	F1	1·9622 (2)		
	F2	1·8888 (4)	F—Co	2·0344 (4)
	F2	2·2527 (4)		
F1—F2		2·7235 (3)		
			F—F	2·8771 (3)
F2—F2		2·9397 (6)		
F1—K		2·9285 (3)		
			F—K	2·8771 (3)
F2—K		2·8585 (3)		

Atomic charges

The net charges on each atom, given in Table 5, were determined by the $\Delta\rho$ partitioning method of Hirshfeld (1977). This has been shown to be a useful method for determining effective charges (Maslen & Spackman, 1985).

In one respect these differ strongly from quantities related to oxidation states, and from observations by other workers (*e.g.* Hirshfeld & Hope, 1980; Baert, Coppens, Stevens & Devos, 1982); the charge of F1 is positive. This is surprising since F is a strongly

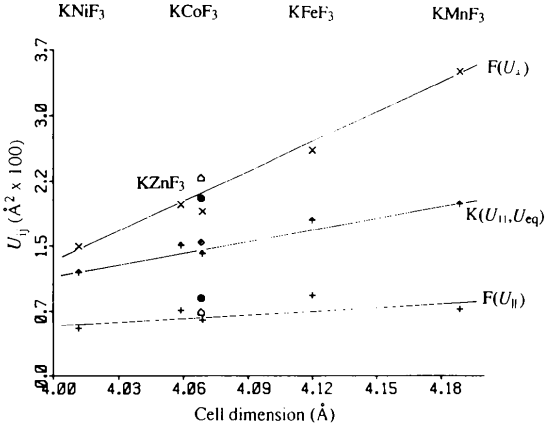

Fig. 2. Thermal-vibrational amplitudes as a function of cell dimension: $U_{\perp}$ and $U_{\parallel}$ to the F—M bond in KMF_3, F1 (△), F2 (●) in $KCuF_3$; U_{11} for K in KMF_3, U_{eq} of K (◇) in $KCuF_3$.

Table 5. *Atomic charges from the Hirshfeld partitioning of* $\Delta\rho$

Atom	Charge (e)
Cu	0·14 (6)
K	0·07 (6)
F1	0·28 (6)
F2	−0·25 (6)

electronegative atom. Initially an artifact resulting from inaccurate extinction corrections was suspected. However, similar results were obtained in study II. It was then noted that Coulomb interaction between static charges as in Table 5 accounts for the changes in the F—F and F—K distances described above. Elongation of the K—F1 and F2—F2 vectors is consistent with repulsive interaction between atoms carrying like charges. Reduction of the K—F2 and F1—F2 distances can be attributed to attraction between charges of opposite sign.

The Cu—F1—Cu distance of 3·9244 (4) Å is shorter than the ideal value of 4·0678 (3) Å. As that distance contracts the depleting effect of the quantum-mechanical interference terms owing to overlap of electrons with parallel spins (*i.e.* of exchange) dominates, generating the positive charge of the F1 atom. The Cu—F2—Cu distance is extended by Jahn–Teller elongation of one Cu—F2 bond, allowing Cu to vibrate maximally in the (001) plane, and least in the [001] direction. The largest mean-square amplitude for F2 of 0·02058 Å^2 is normal to the Cu—F2 bond, but within the (001) plane. Jahn–Teller contraction of the other Cu—F2 vector reduces its length to 1·8888 (4) Å. The Cu—F1 vector, which in a weakly perturbed moiety should have the same length as the short Cu—F2, is reduced only to 1·9622 (2) Å because the structure is tightly packed in the [001] direction. There is no compensating extension of the *c* axis by Jahn–Teller elongation elsewhere in the structure. This is the essential difference from the structural geometry in the (001) plane.

In this context F1 and F2 resemble Cl, which exhibits a full range of oxidation states, since in solution hypochlorites, ClO^- (+1), chlorites, ClO_2^- (+3), chlorates, ClO_3^- (+5), and perchlorates, ClO_4^- (+7), are known in addition to the more common chloride (−1). Of the equivalent series for F, HFO has been reported, giving an effective oxidation state of +1 for F (Studier & Appelman, 1971). Standard texts such as Cotton & Wilkinson (1988) also list hypofluorites. The chemistry of ClO^- (+1) is known only in dilute aqueous solution. It disproportionates rapidly at high concentration above room temperature. This contrasts with ClO_2^- (+3), which has high stability in alkaline solution. Environment affects the charge on halogens, which is clearly relevant to the case of F1.

Maslen & Spadaccini (1989) report trends in the cubic KMF_3 series related linearly to cell size. With the reduction in cell dimension from Mn to Ni the density near *M* is polarized more strongly; the effective atomic charges increase and the amplitudes of thermal motion decrease.

The modulation of interatomic distances by Coulombic interactions between static charges in $KCuF_3$ must also affect the cubic KMF_3 structures. As the 3*d* subshell of the *M* atom fills, greater overlap with the F atoms increases spin conflict. The contribution from antibonding orbitals increases, and the electron density is depleted more strongly from the region near the transition metal. This increased exchange polarization generates the higher atomic charges, and the structure becomes increasingly *ionic*. The Coulombic interactions between charges of opposite sign compact the unit cell, constraining the atoms and dampening their thermal motion. This accounts for the relationships between cell size, temperature-factor coefficients and atomic charges observed for the KMF_3 series.

Difference density

The $\Delta\rho$ sections containing the Cu—F interaction vectors in the (001) plane and in the (110) plane are displayed in Figs. 3 and 4, respectively. The maps for the current analysis are denoted (*a*), with those of study II denoted (*b*). The broad topologies of the maps (*a*) and (*b*) are equivalent in spite of different methods of crystal growth and independent data measurement.

The optimal evaluation of $\Delta\rho$ using extinction-affected data requires careful analysis of the form of correction. The method of Larson (1970) was preferred to others for reasons given by Buttner & Spadaccini (1990). In this analysis there is a high proportion of moderately strong reflections for which extinction, although small, is significant. The modest corrections, which have an appreciable effect on the density, are sensitive to the extinction model. For this reason an independent check of the validity of these $\Delta\rho$ maps is desirable. $\Delta\rho$ in the Tutton salt diammonium hexaaquacopper(II) sulfate, studied by Maslen, Watson & Moore (1987), depends less strongly on the extinction model and is therefore suitable for comparison. The topology near the Cu atom in the Cu—O7—O9 plane for that compound is remarkably similar to that near the Cu atom in Fig. 3(*a*). Both show the features characteristic of a Jahn–Teller distorted Cu^{II} atom.

The main features common to maps (*a*) and (*b*) of Figs. 3 and 4 are:

(i) Strong depletion *ca* 0·5 Å from Cu along the short Cu—F2 bond.

(ii) Depletion, less strong than in (i), 0·25 Å from Cu along the long Cu—F2 bond.

(iii) Extended depletion along the Cu—F1—Cu vector.

(iv) Excess density near the long Cu—F2 contact.

(v) A characteristic feature 'X' at the structural cavity as in other perovskites (Maslen & Spadaccini, 1989; Buttner & Maslen, 1988).

There are some dissimilar features, notably:

(i) Far more density near the short Cu—F2 bond in Fig. 3(*b*) although polarization near F2 itself is more limited. (The magnitude of this broad area of positive density is exaggerated by a ripple caused by the two strongest reflections, which are inadequately corrected for extinction. The reflections were included for the sake of completeness. Their contribution to the $\Delta\rho$ is easily discerned from its characteristic shape.)

(ii) A large peak at 0·45 Å from F2 along the long Cu—F2 bond in Fig. 3(*a*) and smaller differences which nevertheless do not disguise the qualitative agreement between the $\Delta\rho$ maps for the two studies.

The radial dependence of $\Delta\rho$ near the Cu has features characteristic of $\Delta\rho$ maps for ideal low- and high-spin structures. In the high-spin case the depletion of density is closer to the nucleus than in the low-spin case. The depletion closest to the Cu atom is $-1{\cdot}15$ e Å^{-3} at 0·25 Å and there is an outer depletion of $-1{\cdot}56$ e Å^{-3} at 0·48 Å (Fig. 3*a*), the distances being measured from the Cu nucleus.

Because of the high occupancy of the Cu atom's 3*d* subshell, electron density is depleted when the atom overlaps with the electron density of the ligands. This is a well-known effect of exchange (antisymmetizing of the state functions for identical fermions), which is also responsible for the Pauli exclusion principle. The outer depletion, located

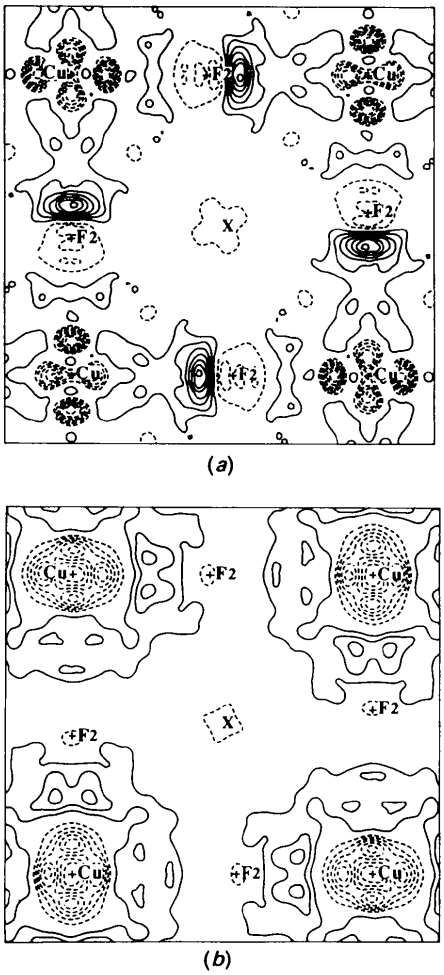

Fig. 3. $\Delta\rho$ maps for the (001) plane in $KCuF_3$: (*a*) current analysis, (*b*) results of study II. Map borders 6·0 by 6·0 Å; contour intervals 0·2 e Å^{-3}; positive, negative contours – solid, short dashes, respectively.

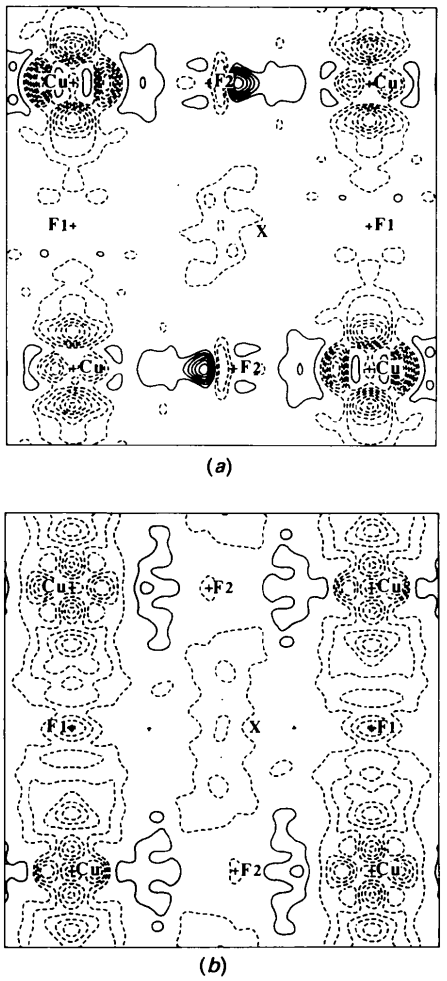

Fig. 4. $\Delta\rho$ maps for the (110) plane in $KCuF_3$: (*a*) current analysis, (*b*) results of study II. Map borders and contouring as in Fig. 3.

along the shortest Cu—F bond where maximum exchange is expected, is typical of depletion of paired spin density. In contrast with this, the depletion close to the nucleus is more typical of that observed near the longer bonds of high-spin structures.

The highest $\Delta\rho$ peak of 1·61 e Å^{-3} is 0·45 Å from F2 (Fig. 3*a*). Because this peak is barely discernible in Fig. 3(*b*) it might be regarded as an artifact of the analysis. However, it is consistent with lone-pair development in the space created by the displacement of F2, and its distance from the F nucleus agrees with values of 0·4 Å for N and O lone pairs described by Dunitz & Seiler (1983). To improve the comparison of these new results with those in study II, the reflections removed by truncation in study I were also removed from the current data. After refinement ($R = 0{\cdot}014$, $wR = 0{\cdot}014$) the peak in $\Delta\rho$ reduced to 1·17 e Å^{-3}, although the map retained the same general topology. The strong effect of truncation on the height of this feature demonstrates the importance of retaining all usable information when evaluating difference densities. It should be emphasized that a phase error for weak reflections with $F_o < F_c$ does not generate a term with the wrong sign in the difference map. The magnitude of the term is $2|F_o|$ lower than its true value. Inclusion of these reflections when evaluating $\Delta\rho$ is a failsafe procedure unless $\sigma(F_o)$ for the reflection is inordinately large.

The difference density in the section containing the Cu and F atoms is shown in greater detail in Fig. 5(*a*). The density close to F2 requires careful study to ensure correct understanding. Progressing from the lone-pair feature in Fig. 5(*a*) toward F2, $\Delta\rho$ drops to $-0{\cdot}63$ e Å^{-3} at 0·12 Å before the nucleus (the F2 nucleus being on a $-0{\cdot}24$ e Å^{-3} contour), rises almost to zero just past (<0·1 Å), decreases to $-0{\cdot}44$ e Å^{-3} at 0·31 Å, and then rises to a ridge of 0·30 e Å^{-3} flanked by peaks of 0·47 e Å^{-3} at 0·75 Å. Thus, in addition to an outer dipole related to the lone pair, there is polarization with a reversed dipole close to the core region.

The large feature in the difference density near F2 contrasts with the flat topology in the corresponding region of density near F1 as shown in Fig. 4(*a*). In contrast with the map near F2, a dipolar contribution to $\Delta\rho$ around F1 is precluded by symmetry. Dipole terms are expected to dominate the polarizability for atoms such as F, with unfilled *p* states. Strongly polarized density near F2 and weakly polarized density near F1 is consistent with the chemical properties of the F atom.

By symmetry, there can be no net force on the Cu atom. Considering the Cu—F2—Cu system as a sum of dipole interactions, with Cu—F2 short and Cu—F2 long, the IAM results in a net force on the F2 nucleus directed towards the lone-pair feature. As pointed out by Spackman & Maslen (1985), nuclear equilibrium is achieved by polarization close (<0·4 Å) to the nuclear position with density further away playing a minor role. The polarization close to the nucleus in Fig. 5(*a*) counteracts the repulsion between the nuclei described above. As already noted, high-angle refinement yields a positional parameter $x = 0{\cdot}22745$ (6) compared to the $x = 0{\cdot}22803$ (7) used to evaluate the structure factors for generating $\Delta\rho$ in Fig 5(*a*). The $\Delta\rho$ map for the (001) plane evaluated with $x = 0{\cdot}22745$, refining the other parameters and including all data, is displayed in Fig. 5(*b*). The polarization near the core has been removed, leaving only the lone-pair dipole, which is in the direction opposite to that required to counteract the mutual repulsion of the nuclei. This is a physically unacceptable model for the structure. The difference between the two refinements illustrates how weights of the measurements can alter the bias

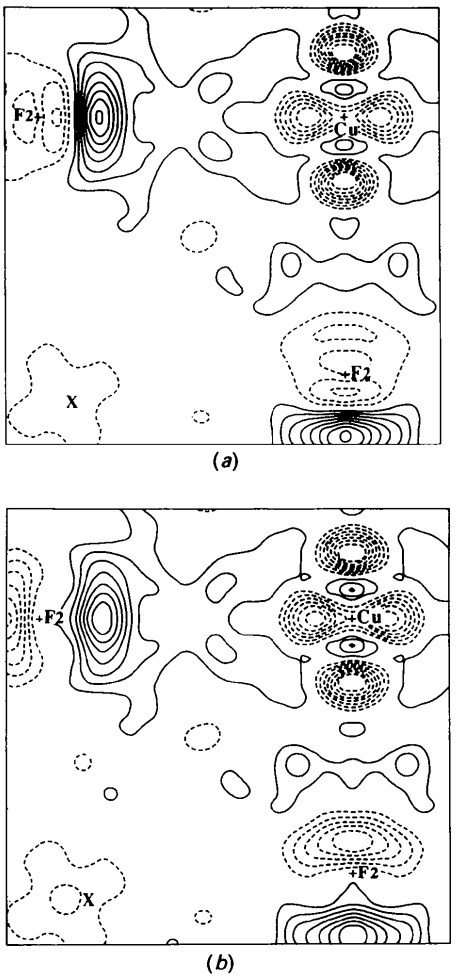

Fig. 5. $\Delta\rho$ maps for the (001) plane in $KCuF_3$: (*a*) current analysis, (*b*) current analysis but with $x = 0{\cdot}22745$ (6). Map borders 3·2 by 3·2 Å. Contouring as in Fig. 3.

of coordinates, owing to atom distortion by chemical bonding, in the least-squares procedure. The simplicity of this structure, with just one general coordinate, provides a simple test of the reliability of high-angle refinement. In this test case it is less satisfactory than that derived from the full data set.

The depletion marked 'X' Figs. 3(*a*) and 5(*a*) has a topology broadly compatible with that for the ideal perovskite $KCoF_3$. There is strong correlation of $\Delta\rho$ at 'X' with cell size (Maslen & Spadaccini, 1989). In Fig. 3(*a*) it reaches a minimum value of $-0{\cdot}37$ e Å^{-3}, compared with $-0{\cdot}43$ e Å^{-3} for the cobalt compound. This reflects the close similarity of the size of the $KCoF_3$ cell with the equivalent cubic cell for $KCuF_3$. However, in Fig. 4(*a*) there is a distinct change from the shape typical of the cubic perovskites. There are nearest-neighbour Cu—Cu distances with two different lengths [4·1415 (4), 3·9244 (5) Å]. The change in shape of the depleted region correlates with the change in position of the F atoms. The depletion is deeper and more extended between the F2 atoms which are closer to one another. This dependence of the shape on F—F distance is not surprising since the F atoms are a factor of approximately $1/\sqrt{2}$ closer to the region than are the Cu atoms.

The feature at 'X' is observed to vary linearly with cell dimension from a peak of 0·5 e Å^{-3} in $KMnF_3$ to a depletion of $-0{\cdot}8$ e Å^{-3} in $KNiF_3$ (Maslen & Spadaccini, 1989). This is a secondary effect originating from the increasingly repulsive exchange between the 3*d* subshell and F-atom orbitals noted above. The exchange term in the Mn—F overlap region for $KMnF_3$ is largely *bonding*, but results in low atomic charges. The atoms retain their essentially neutral character. In the region 'X' where F atoms overlap, additional electrons may be accommodated since the overlap involves open shells. The electron density can move towards that region without conflicting with the exclusion principle. The other extreme, $KNiF_3$, has more *ionic* character. F is closer to the classical closed shell ion. Overlap between negatively charged F atoms involves mainly paired spin electrons. In accordance with the Pauli exclusion principle electron density is depleted from the overlap region. Obviously the *M* atoms play only a minor role in the feature's topology, as noted by Buttner & Maslen (1988). This must also hold for the diffuse 4*s* orbitals of the K atom.

One of us (RHB) wishes to thank the Crystallography Centre of the University of Western Australia for the use of its facilities, NS gratefully acknowledges Professor Marumo for supplying data. The authors wish to thank Associate Professor A. H. White for his invaluable advice and assistance during data measurement. Financial support from the Australian Research Scheme is gratefully acknowledged.

References

ALCOCK, N. W. (1974). *Acta Cryst.* A**30**, 332–335.

BAERT, F., COPPENS, P., STEVENS, E. D. & DEVOS, L. (1982). *Acta Cryst.* A**38**, 143–151.

BECKER, P. J. & COPPENS, P. (1974). *Acta Cryst.* A**30**, 129–147.

BUTTNER, R. H. & MASLEN, E. N. (1988). *Acta Cryst.* C**44**, 1707–1709.

BUTTNER, R. H., MASLEN, E. N. & SPADACCINI, N. (1990). *Acta Cryst.* B. Submitted.

BUTTNER, R. H. & SPADACCINI, N. (1990). *Acta Cryst.* In preparation.

COTTON, F. A. & WILKINSON, G. (1988). *Advanced Inorganic Chemistry*, 5th ed., p. 565. New York: John Wiley.

CROMER, D. T. & LIBERMAN, D. (1970). *J. Chem. Phys.* **53**, 1891–1898.

CROMER, D. T. & MANN, J. B. (1968). *Acta Cryst.* A**24**, 321–324.

DUNITZ, J. D. & SEILER, P. (1983). *J. Am. Chem. Soc.* **105**, 7056–7058.

HALL, S. R. & STEWART, J. M. (1988). Editors. *XTAL2.4 User's Manual.* Univ. of Western Australia, Australia, and Univ. of Maryland, USA.

HIRSHFELD, F. L. (1977). *Isr. J. Chem.* **16**, 198–201.

HIRSHFELD, F. L. & HOPE, H. (1980). *Acta Cryst* B**36**, 406–415.

HUTCHING, M. T., SAMUELSEN, E. J., SHIRANE, G. & HIRAKAWA, K. (1969). *Phys. Rev.* **188**, 919–923.

LARSON, A. C. (1970). *Crystallographic Computing*, edited by F. R. AHMED. Munksgaard: Copenhagen.

KADOTA, S., YAMADA, I., YONEYAMA, S. & HIRAKAWA, K. (1967). *J. Phys. Soc. Jpn*, **23**, 751–756.

KANAMORI, J. (1960). *J. Appl. Phys.* **31**(Suppl.), 14S–23S.

KIJIMA, N., TANAKA, K. & MARUMO, F. (1981). *Acta Cryst.* B**37**, 545–548.

KIJIMA, N., TANAKA, K. & MARUMO, F. (1983). *Acta Cryst.* B**39**, 557–561.

MASLEN, E. N. & SPACKMAN, M. A. (1985). *Aust. J. Phys.* **38**, 273–287.

MASLEN, E. N. & SPADACCINI, N. (1989). *Acta Cryst.* B**45**, 45–52.

MASLEN, E. N., WATSON, K. J. & MOORE, F. H. (1987). *Acta Cryst.* B**44**, 102–107.

MIYATA, N., TANAKA, K. & MARUMO, F. (1983). *Acta Cryst.* B**39**, 561–564.

OKAZAKI, A. (1969*a*). *J. Phys. Soc. Jpn*, **26**, 870.

OKAZAKI, A. (1969*b*). *J. Phys. Soc. Jpn*, **27**, 518.

SPACKMAN, M. A. & MASLEN, E. N. (1985). *Acta Cryst.* A**41**, 347–353.

SPADACCINI, N. (1988). PhD Thesis, Univ. of Western Australia, Australia.

STUDIER, M. H. & APPELMAN, E. H. (1971). *J. Am. Chem. Soc.* **93**, 2349–2351.

TANAKA, K., KONISHI, M. & MARUMO, F. (1979). *Acta Cryst.* B**35**, 1303–1308.

TANAKA, K. & MARUMO, F. (1982). *Acta Cryst.* B**38**, 1422–1427.